*Egypt. J. Chem.* **Vol. 68,** SI: Z. M. Nofal, pp. 399- 416 (2025)

**Egyptian Journal of Chemistry**

**http://ejchem.journals.ekb.eg/**

# Development of Active Modified Kaolin As Anticorrosive Fillers

**Walaa W. Diab*[1], Yasser K. Abdel-Monem[2], Nabil A. Abdel Ghany[3], Ahmad M. Labeeb[4] , Hassan S. Emira[1] and Yosreya M. Abu Ayana[1]**

[1] Polymers and Pigments Department, Chemical Industries Institute, National Research Centre, 33 Bohouth Street, Dokki, Giza, Egypt, PO Box 12622.

[2] Chemistry Department, Faculty of Science, Menoufia University, Shibin El Kom, Egypt.

[3] Physical Chemistry Department, Electrochem. and Corrosion Lab**,** National Research Centre, 33 Bohouth Street, Dokki, Giza, Egypt, PO Box 12622.

[4] Liquid Crystals Laboratory, Microwave Physics and Dielectrics Department, Physics Research Institute, National Research Centre, 33 Bohouth Street, Dokki, Giza, Egypt, PO Box12622.

**Abstract**

Intercalation of kaolin by urea molecules via mechanical grinding resulted in partial delamination with some broken bonds between kaolin layers. This permits subsequent modification by either active APTES (3-amino propyl triethoxy silane) or urea-formaldehyde polymer chains. Therefore, this study aims to develop new active fillers thatdepend on modified kaolin and encapsulated modified kaolin, which are considered new encapsulated corrosion inhibitors. A type of these encapsulated active fillers, the intercalated kaolin by urea **(UK)** was silylated with APTES and then coated by a shell of urea-formaldehyde polymer through an in-situ polymerization method. Another type, UK, was modified by urea-formaldehyde polymer and then coated by an APTES layer. All the prepared fillers were characterized by FTIR, X-ray diffraction, thermal analysis, SEM, and EDX measurements. Then, varnish formulations containing 10% of prepared fillers and alkyd resin were coated on mild steel surfaces to study their efficiency as anticorrosive fillers by electrochemical impedance spectroscopy (EIS). The results indicated that APTES was successfully grafted onto the surface of kaolin and in between its exfoliated layers, and urea-formaldehyde polymer formed a continuous shell encapsulating the active silylated kaolin molecules. Additionally, the encapsulated filler UK-UF-AP has superior anticorrosive properties for steel protection.

**Keywords**:
Kaolin, mechanochemical grinding, urea-formaldehyde, APTES grafting, EIS

## 1. Introduction

Clay minerals have attracted a great attention recently in industrial and environmental protection because they are pristine, easy and available nano-materials[1, 2]. Kaolin is a type of clay mineral which is classified as 1:1 layered alumina/silicate with the chemical formula $Al_4Si_4O_{10}(OH)_8$[3,4]. It has two layer units, one alumina octahedral and one silica tetrahedral. These layers are held together by formed hydrogen bonds between oxygen atoms from the silica layer and hydroxyl groups on the surface of the alumina layer[1,5]. Kaolin is the most popular mineral used as a filler or a pigment in industrial applications such as anticorrosive paint production [3] due to its fine particle size, platy shape, physical and chemical properties, non-toxicity [6], high brightness, surface chemistry and crystal structure characteristics[3,7]. Silylation of kaolin (or silane grafting) is an efficient method of kaolin modification by silane coupling agents to advance its properties (especially anticorrosive properties). Successful silylation depends on the external surface, internal surface and the broken edges of kaolin. Kaolin's Al-octahedral outer hydroxyl groups act as possible active sites for organo-silane grafting reaction on the surface by condensation reaction with alkoxyl groups and/or the hydroxyl groups in the hydrolyzed silane (no need for pre-intercalation) [8]. However, it isn't an easy method to modify the inner hydroxyl groups of kaolin by direct reaction (need pre-intercalation) using large molecules of organo silane like 3-amino propyl triethoxy silane (APTES)[9, 10]. Hence, intercalation of kaolin is a successful strategy to obtainaneasy path or reactive sites at the inner surface. The intercalation takes place through many of mechanisms, depending on the region of reaction between organo-molecules and the kaolin surface. The active guest molecule enters between the stacked kaolin layers to separate them apart. Therefore, breaking the H-bonds between the OH groups of the octahedral layer and the oxygen atoms of the siloxane tetrahedral layer is necessary[1,7]. Intercalation of kaolin layers with

*Corresponding author e-mail: walladiab@yahoo.com.; (**Walaa W. Diab**).
Received date 19 April 2025; Revised date 06 May 2025; Accepted date 21 May 2025
DOI: 10.21608/EJCHEM.2025.376873.11623

organic molecules can create novel bonds with the hydrophobic siloxane layer and/or with the hydrophilic hydroxyl group in the octahedral layer[1]. Active organic molecules can be separated into two groups. Group 1 contains organic molecules (such as urea, hydrazine, formamide and acetamide) that can form strong H-bonds with the siloxane layer of kaolin as studied in this paper. Group 2 contains organic molecules with strong dipole moments (such as dimethylsulphoxide "DMSO" and pyridine-N-oxide) that can also react with the siloxane layer[5,9]. Mechanochemical intercalation -or by other words- dry grinding of kaolin with active urea molecules causes intercalation of kaolin's layers in order to generate many broken bonds or active sites in the interlayer space of kaolin [11,12] to provide such opportunity for silane agents (for example) to react under mild conditions. Insertion of urea molecules may be through the $NH_2$ groups' reaction (as H-donors) –possible forming weak H-bonding with the inner OH groups or reacting with the oxygen atoms at the tetrahedral layers-as well as the carbonyl groups' reaction (H-acceptors) with hydroxyls of the octahedral layer forming H-bonds[1,7]. Encapsulation of kaolin is an achievable technology to control active ingredients release through the shell in the applied field media. Since interest in self-healing corrosion protection coatings has increased, it has been used. Fast recovery of the corrosive regions in metal substrate could happen by rupture of capsule walls incorporated in a coat and releasing active components inside[13,14]. Obviously, in most literature, the capsule wall material consists of amino resins such as urea or melamine formaldehyde polymer with regarding to the material availability, economy and cheap raw materials[15-17]. When silylated kaolin with functional groups, such as amino or mercapto and alkoxy groups, reacts with the polymer, a network of covalent bonds is formed between the polymer chains, kaolin, and silane coupling agents. This significantly improves the characteristics of the resulting kaolin polymer nanocomposites[10,15]. Mild steel is recognized as the most metal that has exceptional qualities, environmental solidity or resistance, low cost and accessibility[18]. Hence, it is commonly used in many sectors, such as manufacturing, marine and transportation. Steel suffers from the extended corrosion problem like pickling, acidizing etc., during industrial processes. Encapsulated corrosion inhibitors act as a key function for solving the steel corrosion problem with their unique properties [19-23]. Xiang Liu et al. (2022)[24] used an electrochemical method for fast hydrophobic modification of kaolin applied in corrosion protection for magnesium alloys study. Zhe Li et al. (2022)[25] developed an anticorrosive coating with antibacterial ability by means of urea-formaldehyde resin. Mahdavi F., et al. (2014)[12] used a dry grinding technique to intercalate urea molecules inside a kaolin layer as preparation for controlled release fertilizer. In the field of corrosion inhibition studies, this research is a supplementary contribution to the work of other earlier authors. Advancing new active fillers based on kaolin, modified kaolin, and encapsulated kaolin is the main objective of this paper study. These active fillers were added to alkyd varnish coating to protect steel from corrosion. The performance of steel protection was investigated by EIS compared with using a reference pigment known with its anticorrosive properties

## 2. Materials and Experimental Techniques

### 2.1. Materials

Urea supplied from El-Nasr Pharmaceutical Chemicals Company, Cairo, Egypt.Formaldehyde solution (liquid 34-38%) (Formalin)manufactured and packed by PIOCHEM Company for laboratory chemicals, Cairo, Egypt.Ethanol absolute ≥99.8% supplied from Sigma Aldrich. Sodium carbonate anhydrous (Soda ash) supplied from El-Nasr Pharmaceutical Chemicals Company, Cairo, Egypt.Kaolin (Aluminum silicates) white powder supplied from Riedel-deHaen brand, Germany.Citric acid (monohydrate) supplied from El-Nasr Pharmaceutical Chemicals Company, Cairo, Egypt.Propan-2-ol (Isopropyl alcohol ≥ 99.5%) supplied from Fisher Scientific Chemicals Company, USA.Tetra ethyl orthosilicate (TEOS)supplied from Sigma Aldrich. 3- (Triethoxy silyl)-propyl amine (APTES) ≥98% supplied from Sigma Aldrich. Alkyd resin (KRMO-100/60WS) was provided by KAPCI coatings, Egypt. Zinc phosphate (ZP) was supplied from BASF, Germany.
**Note**: Zinc phosphate (ZP) is known by its high anticorrosive properties and promotes the adhesion of coating. It was used in this paper as a reference pigment in varnish formulations to study the efficiency of the new active prepared fillers via EIS measurement. In brief, we aimed to advancing the prepared fillers' anticorrosive properties to be similar to the anticorrosive properties of ZP[26-29].

### 2.2. Experimental Techniques

#### 2.2.1. Washing of Kaolin

Washing of kaolin from impurities was done by a wet soaking method in warmed distilled water described by Aroke et al. (2013)[30]. 100 gm of kaolin sample was soaked in 1liter of warmed distilled water for 48 hr. The distilled water was decanted; washed kaolin was dried in 100°C for 3 days and was symbolized by **K**.

#### 2.2.2. Intercalation of Kaolin by urea[7]

A mixture of dried washed kaolin and solid urea in a 1:1 weight ratio was ground by dry grinding (mechanochemical intercalation) process for 2 hr. The mechanochemical activation (e.g., dry grinding) of kaolin increases the surface area, ion-exchange capacity, crystal structural deformation and intercalation reactivity. The dry grinding was carried out by a Retsch-laboratory planetary mill. The rotation speed was 375 rpm. Then, the obtained mixture was washed with isopropanol several times to remove excess urea, dried at 90°C for 48 hr. and symbolized by **UK.**

#### 2.2.3. Modification of urea-intercalated kaolin (UK)

Four samples were prepared based on intercalated kaolin (UK) as follows:

***(A) Modification of urea-intercalated kaolin by silane coupling agent (APTES)***

Intercalated kaolin **UK**(2 gm) was dispersed in 50 ml of anhydrous ethanol in a 250 ml three-necked round flask and was stirred for 1 hr. at room temperature. Ammonia (5-20 ml) was added to the mixture and was stirred for another 1 hr. at 60°C

(pH=7.5-8). TEOS (5 ml) was being inserted gradually into the solution with constant stirring at 60°C for 6 hr. The solution was filtered and washed several times with ethanol.
The previous residue was dispersed in 50 ml of anhydrous ethanol. Hydrolyzed APTES (2-6 gm) was added drop-wise with continuous stirring for 2 hr at 80°C. The solution was filtered, washed several times and dried for 24 hr. at 110°C. The product was denoted by **UK-AP**.
NOTE: Treatment the UK first with TEOS coupling agent (with its small molecules) as an intermediate step for the intercalation. TEOS gives more opportunities for grafting APTES silane coupling agents inside kaolin layers with free functional groups of urea. Additionally, providing more Si-OH bonds inside, at edges and on the surface of kaolin for APTES (with its large molecules) to be grafted[8, 24, 31].

***(B) Encapsulating the UK by urea-formaldehyde (UF) polymer***

Step 1: weight ratio of 1:2 urea to formaldehyde were placed in three necked baffled stainless steel tank reactor capacity of 250 ml. The pH of the mixture was adjusted to 8-9 with sodium carbonate (1N), stirred using a mechanical stirrer at 300 rpm, for 30 min. at 75°C to prepare UF pre-polymer (methylol-UF).
Step 2:A pre-determined amount of UK was dispersed in a mixture of poly vinyl alcohol (PVA) solution and sodium lauryl sulphate solutions. The mixture was stirred vigorously in a homogenizer for 15 min.
The mixed UK solution was added drop-wise to the methylol-UF solution with vigorous continuous stirring at 75°C for 10 min., followed by adding distilled water while stirring is continuous for 30 min.
Step 3: The previous solution pH was adjusted by citric acid solution to 3.5-4 to complete the polymerization step with continuously stirring at 75°C for 2 hr. The encapsulated powder could be obtained by centrifuge (2500 rpm, 5 min. at room temperature). The encapsulated powder was washed several times with distilled water and dried at 90-100°C for 48 hr. The product was symbolized by **UK-UF**.

***(C) Encapsulating of UK-AP by urea-formaldehyde (UF) polymer***

Encapsulating of UK-AP was following the same steps as described before in (B) but in this case, UK-AP was used instead of UK. The product was symbolized by **UK-AP-UF.**

***(D) Encapsulating of UK by urea-formaldehyde (UF) polymer followed by APTES silane coupling agent***

Both steps 1 and 2 were carried out as similarly as those procedures in (B) preparation until step 3inwhich; the mixed UK solution's pH was adjusted to 5-5.5 with citric acid solution with continuous stirring at 75°C for 30 min. APTES was added to the solution drop-wise with constant stirring for 1 hr. Then, the pH of the solution was adjusted again to 3.5-4 with the same constant stirring at 75$^0$C. The product was donated by **UK-UF-AP**.

**2.2.4. Preparation of varnish formulations**

Eight varnish formulations were prepared based on a 10% concentration of the prepared active fillers (ZP as reference, K, UK, UK-AP, UK-AP-UF, UK-UF and UK-UF-AP) and alkyd resin. These formulations were prepared to study the efficiency of these active fillers as anticorrosive fillers compared with ZP pigment. All ingredients were mixed with solvent by the appropriate quantity using a dispersing machine in order to obtain the desirable varnish mixture with a proper consistency (ASTM D 1210-05:2022)[32]. This varnish mixture was coated on mild steel (MS) panels by a film applicator to finally obtain a dry film with a 120 ± 5 μm thickness[33]. Table (1) indicates the varnish formulations used in the coating system.

Table (1): the constituents of the prepared varnish formulations

| Component | F1(g)% | F2(g)% | F3(g)% | F4(g)% | F5(g)% | F6(g)% | F7 (g)% | F8 (g)% |
|---|---|---|---|---|---|---|---|---|
| **Alkyd resin (60%)** | 89.3 | 82 | 82 | 82 | 82 | 82 | 82 | 82 |
| **Cobalt Octoate (12%)** | 10.7 | 9.8 | 9.8 | 9.8 | 9.8 | 9.8 | 9.8 | 9.8 |
| **ZP** | ----- | 8.2 | ----- | ----- | ----- | ----- | ---- | ---- |
| **K** | ----- | ---- | 8.2 | ----- | ----- | ----- | ---- | ---- |
| **UK** | ----- | ----- | ----- | 8.2 | ----- | ----- | ---- | ---- |
| **UK-AP** | ----- | ----- | ----- | ----- | 8.2 | ----- | ---- | ---- |
| **UK-AP-UF** | ----- | ----- | ----- | ----- | ----- | 8.2 | ---- | ---- |
| **UK-UF** | ----- | ----- | ----- | ----- | ----- | ----- | 8.2 | ---- |
| **UK-UF-AP** | ----- | ----- | ----- | ----- | ------ | ----- | ----- | 8.2 |
| **Total** | 100 | 100 | 100 | 100 | 100 | 100 | 100 | 100 |

**2. 3. Characterization**

***2.3.1 X-Ray Diffraction Analysis (XRD)***

Interlayer spacing of all prepared samples was determined by X-ray diffraction using (a Shimadzu 600). X-ray diffraction patterns between 2θ of 2° to 10° were obtained at a scan rate of 2° min$^{-1}$ by X-ray irradiation of a Cu Kα tube having wavelength of 0.1546 nm by a generator voltage of 40 kV, and a generated current of 40 mA at room temperature.

***2.3.2. Fourier Transforms Infrared Spectroscopic Analysis (FTIR)***
FTIR spectra were obtained using a Bruker Vertex 80 (Germany) combined by a platinum diamond comprises ATR. A diamond disk is with an internal reflector in the range 4000-400 $cm^{-1}$ with resolution 4 $cm^{-1}$ and refractive index 2.4.

***2.3.3. Thermal Analysis***
Prepared samples were investigated through thermogravimetric analysis (TGA) by using a Shimadzu TGA-50 thermogravimetric analyzer, Columbia, EUA, in a nitrogen atmosphere at a 10ºC/min heating rate in the range from room temperature to 1000ºC.

***2.3.4. Energy Dispersive X-Ray Analysis (EDX) and Scanning Electron Microscopy (SEM)***
EDX is used for determining the elemental composition of prepared samples and the morphology of all prepared samples was studied by a Quanta FEG-250 scanning electron microscope.

***2.3.5. Visual corrosion test***
Mild steel panels ($5^x7$ $cm^2$) were used as the substrate for the varnish formulation coating with a desirable thickness. These panels were left to dry for one week at least and then were used in the immersion for corrosion tests. The coated panels were edged by wax to protect the coated area from the edges. A scratch 1mm wide was done by a sharp blade in the coated face area in order to uncover the metal for immersion. The immersion of coated steel panels was in 3.5 wt% sodium chloride (NaCl) solution for 28 days[33]. Degree of rusting and degree of blistering were visually estimated at the end of immersion time (ASTM D610-08:2019 and ASTM D714-02:2017)[34, 35].

***2.3.6. Electrochemical Impedance Spectroscopy (EIS)***
The performance and durability of the coat on mild steel were investigated by EIS in 3.5wt% NaCl solution at room temperature ±25 ºC. The testing cell consists of three-electrodes. The coated steel sample considers the working electrode with a measured area of 4.5 $cm^2$, Ag/AgCl as the reference and Platinum as the auxiliary electrode. The cell connected to Potentiostat/Galvanostat, AUTO LAB 302N, with FRA32, the Netherlands. The spectra were measured at potential (V) connected to open circuit potential (OCP) in a range of frequency 35 to 100 kH[36].

## 3. Results and Discussion
Figures of all prepared samples are divided into three groups in XRD, FTIR and thermal analysis. **Group A** is a comparison between urea molecules (U), washed Kaolin (K) and urea-intercalated kaolin (UK). **Group B** is a comparison between urea-intercalated kaolin (UK), treated UK with APTES silane coupling agent (UK-AP) and treated UK with APTES silane coupling agent and encapsulated by urea-formaldehyde polymer (UK-AP-UF). **Group C** is a comparison between urea-intercalated kaolin (UK), urea-intercalated kaolin encapsulated by urea-formaldehyde polymer (UK-UF) and urea-intercalated kaolin encapsulated by urea-formaldehyde polymer and then by APTES silane coupling agent (UK-UF-AP).

### 3.1.XRD Analysis
XRD patterns of Group A are indicated in Fig. (1). U molecules' XRD pattern profiles show three characteristic peaks: one sharp peak at $2\theta$ 22.42º with *d*-value 3.9623 Aº and two broad peaks at $2\theta$ 24.71º and 31.54º with *d*-values 3.6000 and 2.8431 Aº, respectively. As for raw kaolin XRD patterns, the most specific three peaks appear at $2\theta$ 12.33º, 24.98º and 26.41º with basal $d_{001}$reflection value 7.1776, 3.5613 and 3.3681 Aº, respectively[6, 37]. After dry grinding of raw kaolin with urea molecules, a much broader peak appears at $2\theta$ 8.38º with a basal $d_{001}$reflection value 10.5503 Aº. Also, a peak appears at $2\theta$ 25º with basal $d_{001}$reflection value 3.5609Aº.This change of position from raw kaolin indicates intercalation happened by dry grinding and kaolin layers expanded with the presence of urea molecules, causing structural disorder in kaolin layer stacking[4,7,11,12,38].
In groups B and C, the comparison between XRD patterns in the two groups depends on the basic peaks that appeared in the UK XRD pattern at $2\theta$ 8.38º and $2\theta$ 25º with a remaining stability of other peak values at $2\theta$ 26.6º (d-spacing 3.3269 Aº) , 36.5º (d-spacing 2.4599 Aº) and 39.5 º(d-spacing 2.2823 Aº) (Peaks of K).

Group B is presented in Fig. (2). The XRD pattern of UK-AP indicates shorter intensity and an increase in broadening of the peak at $2\theta$ 8.38º in comparison with the UK pattern. The peak at $2\theta$ 25º shifted to $2\theta$ 24.7º with a basal $d_{001}$reflection value 3.5942 Aº.Silanization of UK, in which APTES reacts and grafts to the surface, edge and probably inside layers, causes more expansion between layers of UK[9].The characteristic peak at$2\theta$ 8.38º seems to have disappeared and the peak at $2\theta$ 25º shifted to $2\theta$ 24º with d-spacing 3.7022 Aº in the UK-AP-UF pattern. This is a proof of coveringUK-AP with a shell of urea-formaldehyde polymer, as free functional groups in treated kaolin (UK-AP) reacted with the polymer, masking kaolin completely[8].
In group C, the XRD pattern of UK-UF shows the same peak at $2\theta$ 8.38º corresponding to UK but with low intensity and broadness(with a stable peak at $2\theta$ 25º),which confirms the encapsulation of UF polymer on the modified UK surface. The UK-UF-AP pattern also shows the same characteristic peak at $2\theta$ 8.38º with much lower intensity and much broader width (with a stable peak at $2\theta$ 25º) compared with UK, which proves the success of APTES molecules in reaction and grafting on the surface of UK-UF[8].

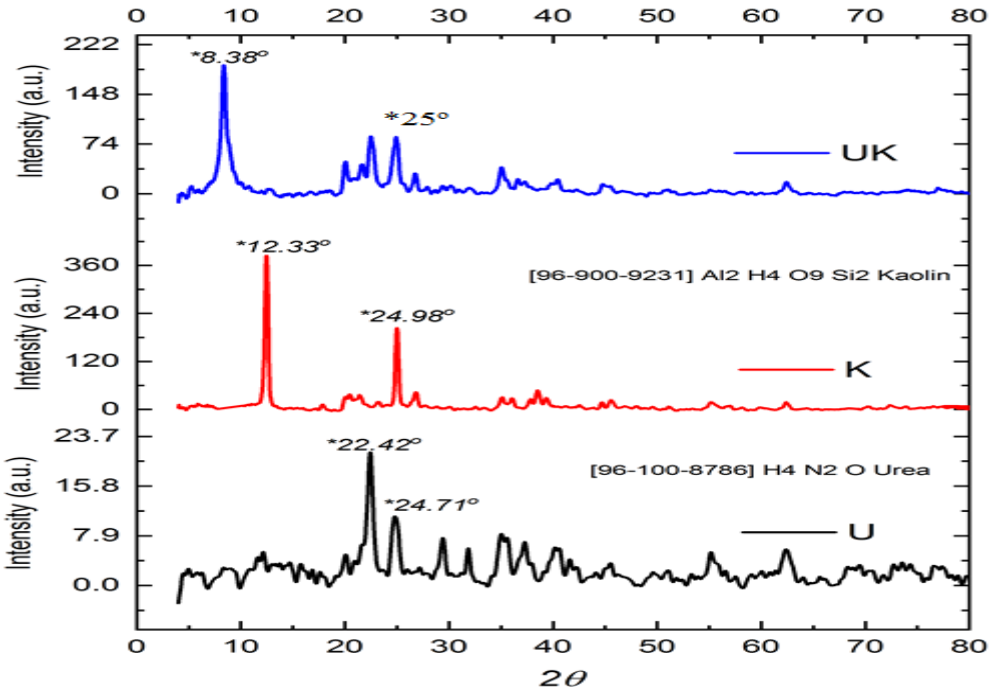


**Fig. 1:** Group (A): XRD patterns of **U**, **K**, and **UK**

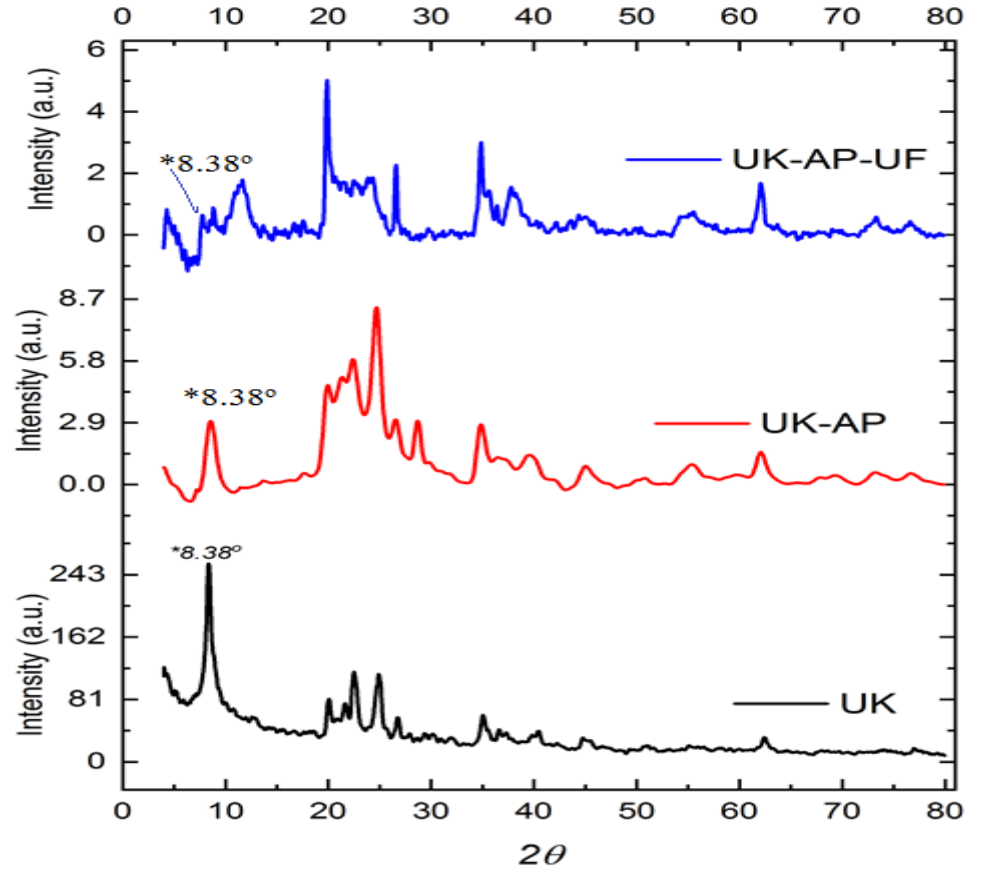


**Fig. 2:** Group (B): XRD patterns of **UK**, **UK-AP**, and **UK-AP-UF**

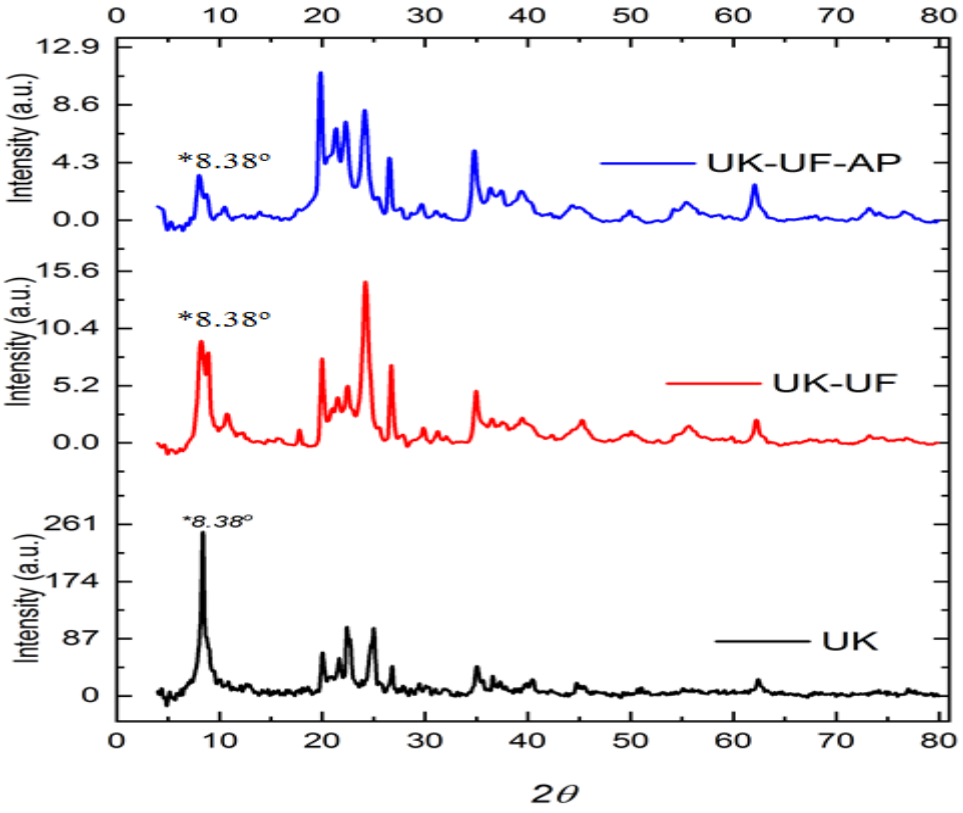


**Fig. 3:** Group (c): XRD patterns of **UK**, **UK-UF**, and **UK-UF-AP**

### 3.2. FTIR Spectroscopic Analysis

Fig. 4 represents the infrared spectra of group A. As for urea molecules (U) spectrum in the high frequency region shows two main important peaks at 3428 and 3328 $cm^{-1}$ representing N-H bond strong stretching vibrations of urea molecules. In the middle frequency region, the spectrum shows one peak at 1674 $cm^{-1}$ corresponding to N-H bond vibration of the amide group of non-bonded urea molecules as presented in Fig. (5a). Two peaks appear at 1590 $cm^{-1}$ belongs to C=O bond stretching vibration and 1460 $cm^{-1}$ belongs to C-N bond anti-symmetric stretching vibration[39].

The infrared spectrum of kaolin **K** shows three main characteristic peaks at 3695, 3650 and 3620 $cm^{-1}$. The peaks at 3695 and 3650 $cm^{-1}$ are assigned to the surface hydroxyl groups (-OH) stretching vibration of the alumina sheet surface. The hydroxyl groups at alumina sheet surfaces are active sites acting as H-donors or acceptors at intercalation reactions forming hydrogen bonds (H-bonds). The peak at 3620 $cm^{-1}$ is related to the stretching vibration of inner –OH groups at the kaolin structure. The bands at 1114, 1030 and 1005 $cm^{-1}$ correspond to Si-O-Si bond anti-symmetric stretching vibration transformations of kaolin. The observed band at 910 $cm^{-1}$ corresponds to Al-O-H bond vibration and bands at 788, 750, 530 $cm^{-1}$ are attributed to the Al-O-Si bond transformations in the structure of kaolin. The peaks in the low frequency region at 685 $cm^{-1}$ corresponds to Mg/Al-OH vibration and those at 460, 425 $cm^{-1}$ correspond to Si-O bending vibrational modes[1,4,7,11, 38].

The infrared spectrum of kaolin intercalated with urea **UK**, in the high frequency region shows a decrease in the intensity of the peak at 3695 $cm^{-1}$ and the peak at 3650 $cm^{-1}$ disappears, which indicates urea intercalation by forming H-bonds between surface –OH groups of kaolin and urea molecules. The peak at 3620 $cm^{-1}$ is still in its place in the high frequency region with lower sharp intensity. This is a proof that the crystal structure of kaolin isn't completely destroyed or changed after dry grinding with urea molecules. Hence, the presence of urea molecules during the dry grinding process for intercalation prevents deformation of the crystal structure of kaolin. Moreover, two new peaks characteristic of the UK spectrum at 3500 and 3410 $cm^{-1}$ (compared with the site of the $NH_2$ group for urea) refer to N-H bond stretching vibrations resulting from interaction between$NH_2$ groups (as H-donors) of urea molecules and kaolin's oxygen of the based tetrahedral layer through H-bonding[1,4,7,11,12].

In the middle frequency region, the peak of the N-H bond of urea shows a shift from 1674 to 1665 $cm^{-1}$ during dry grinding of urea with kaolin. There is a new peak that appears at 1621 $cm^{-1}$ which is attributed to $NH_2$ group deformation vibrations. These two peaks indicate that the interaction of $NH_2$ groups of urea with –OH groups of kaolin. The peaks at 1585 $cm^{-1}$ correspond to C=O group vibration and the peaks at 1472 $cm^{-1}$ correspond to C-N group vibration compared with urea spectra. There is a decrease in the wavenumber of the C=O group and an increase in the wavenumber of the C-N group; these changes prove that the C=O groups of urea molecules are active sites to interact by forming H-bonds with –OH groups of alumina layers for kaolin and respectively strengthen the stretching vibration of C-N groups (shown in Fig. **5**b,c). The peak at

1114 $cm^{-1}$ of pure kaolin spectrum shifts to 1120 $cm^{-1}$ in the UK spectrum due to the urea intercalation reaction. In the low frequency region, the weak intensities of peaks at 788 and 530 $cm^{-1}$ are also evidence for intercalation of urea in kaolin without completely crystal structure deforming or destroying[1,4,7,11,12].

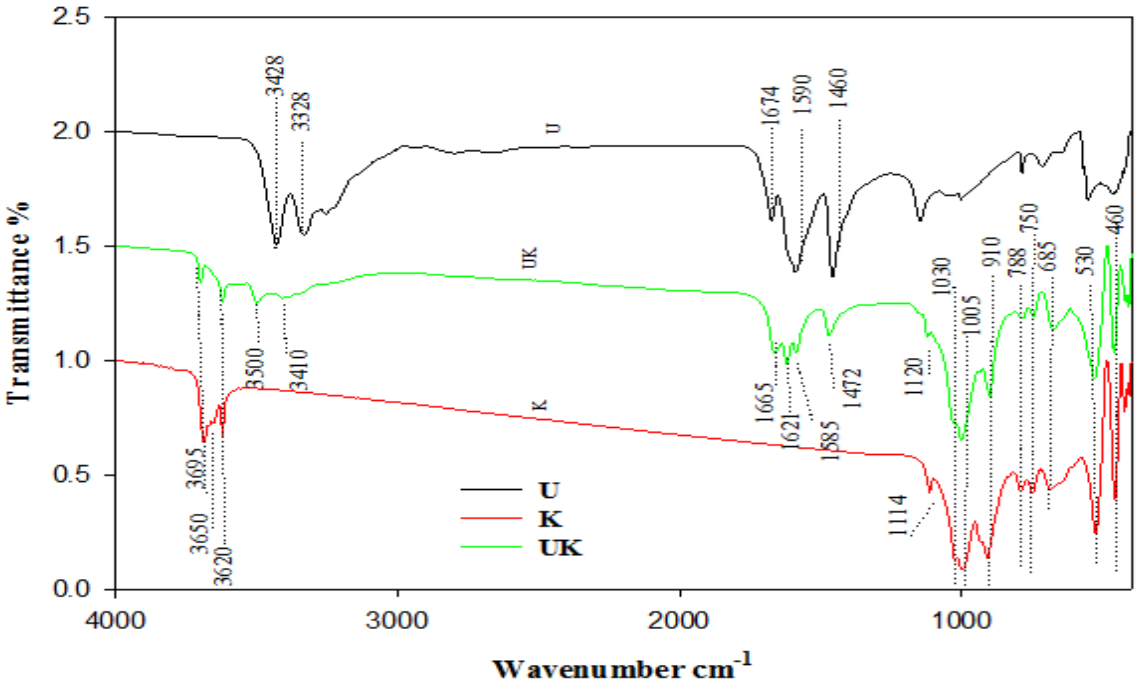


**Fig. 4:** Group (A): FTIR spectra of **U**, **K**, and **UK**

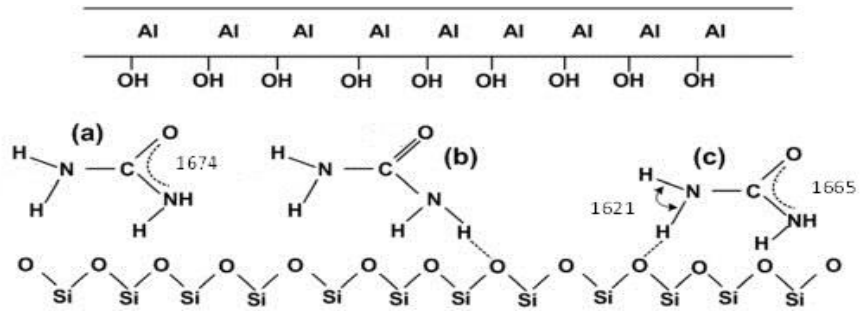


**Fig. 5:** The suggested mechanism of forming H-bonding between urea and kaolin: (a) free non-bonded urea molecules (b) H-bond between urea $NH_2$ group and oxygen of silica layer with free C=O group and (c) H- bond of urea $NH_2$ with oxygen of silica layer after conjugation occurs[7].

Fig. 6 shows the FTIR spectra of group (B). In the high frequency region of the UK-AP spectrum is decreasing in the intensity of the peaks at 3695 $cm^{-1}$ and 3620 $cm^{-1}$ (corresponding to inner –OH groups in kaolin) compared with the UK spectrum. It proves that grafting of APTES silane coupling agent with most available –OH groups of intercalated kaolin with urea. Also, decreasing in intensity at the band 3500 $cm^{-1}$ (which corresponds to –NH group vibration) and the disappearance of the other peak at 3410 $cm^{-1}$ indicate the complete reaction of the APTES silane coupling agent with UK. In the middle region of frequency, the peak of –NH vibration for UK at 1665 $cm^{-1}$ shifts to 1674 $cm^{-1}$ in UK-AP and decreases in intensities. This is a confirmation of a reaction of active –NH groups from intercalated urea inside kaolin layers with APTES silane coupling agent. Moreover, the broadening and low intensity of peaks of Si-O bonds at 1030 and 1005 $cm^{-1}$ prove successful grafting of silane. Decreasing intensity of all peaks representing the C=O bond at 1585 $cm^{-1}$, the C-N bond at 1472 $cm^{-1}$ and the Al-OH bond at 910 $cm^{-1}$ confirms grafting of the APTES silane coupling agent[8,9].

All peaks for UK-AP-UF nearly exist in the same region of frequencies but with low intensities compared with UK and UK-AP peaks. This is due to grafting of the APTES silane coupling agent with most active sites available in the UK, which are coated by urea-formaldehyde polymer as a shell[8].

Fig. 7 represents infrared spectra of group C. The UK-UF spectrum has nearly the same positions as UK with low intensity of –OH and -NH groups. Beaks at 3500 $cm^{-1}$ and 3410 $cm^{-1}$ correspond to the –NH bond of the urea structure having a low intensity at 3410 $cm^{-1}$ and at 3500 $cm^{-1}$ almost disappearing. The peak for C=O shifts from 1585 to 1545 $cm^{-1}$ with low intensity and the peak for C-N at 1472 $cm^{-1}$ nearly disappears. These observations about the UK-UF spectrum confirm that the reaction of free active groups in the urea structure inside kaolin layers with active polymer chains, which formed a coated layer, covered the intercalated kaolin[8].

After treatment of UK-UF with APTES above the shell of urea-formaldehyde polymer, the spectrum of UK-UF-AP is almost similar to the UK-UF spectrum. A change happened to C=O for a low wavenumber and with a low intensity from 1585 $cm^{-1}$ to 1545 $cm^{-1}$. There is an appearance of new peaks corresponding to APTES (silane coupling agent). The new peaks at 2925 and 2855 $cm^{-1}$ are attributed to –CH and $–CH_2$ groups stretching vibration, respectively. Also, a new peak at 1260 $cm^{-1}$ belongs to the Si-C stretching vibration of APTES. These three new peaks are the most characteristic ones for UK-UF-AP spectrum, with increased intensities suggesting that more APTES covered the UK-UF surface[5,8,9].

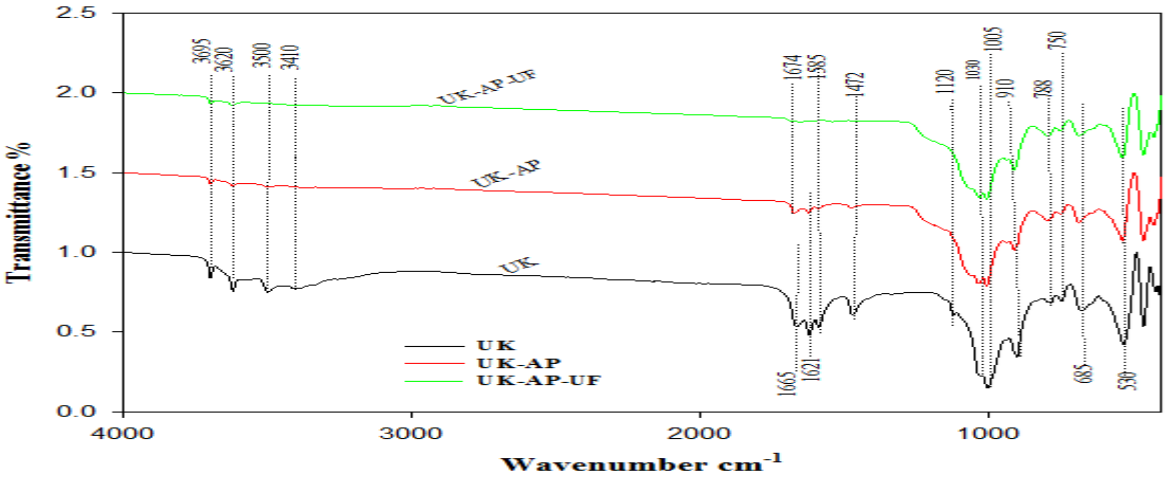


**Fig. 6:** Group (B): FTIR spectra of **UK, UK-AP** and **UK-AP-UF**

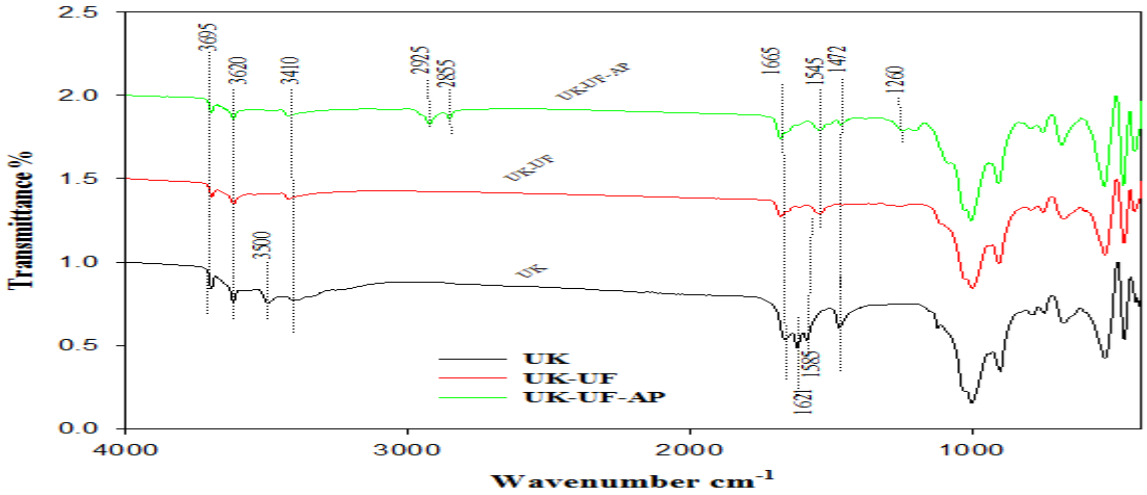


**Fig. 7:** Group (C): FTIR spectra of **UK, UK-UF** and **UK-UF-AP**

### 2.3.3. Thermal analysis TGA

Thermogravimetric analysis generally depends on chemical structure of materials and its nature on forming links such as crosslinks, bond energy is the responsible for thermal stability. Fig. (8, 9 and 10) show the TGA curves, DTA curves and their differences in temperature respectively for all specimens in groups A, B, and C. Table (2) indicate the initial decomposition temperature $T_{initial}$, the final decomposition temperature $T_{final}$ and the maximum peak decomposition temperature $T_{max}$ for prepared specimens.

In Fig. (8), urea molecules (U) generally after the temperature reached to the melting point of urea molecules 133°C gases begin to evolve such as $NH_3$, then molten urea decomposes gradually[40,41] and show two decomposition stages. The first decomposition stage for U molecules starts from 143°C to 267 °C ($T_{max=}$ 246°C), the second decomposition stage starts from 299°C to 481°C ($T_{max=}$ 395°C).

Kaolin (K) curves show one decomposition stage starts from 364ºC to 735ºC ($T_{max=}$ 535ºC) at which the dehydroxylation of kaolin occurs[37].

Urea intercalated kaolin (UK) curves indicate two stages of decomposition. One stage starts from 115ºC to 290ºC ($T_{max=}$ 213ºC), corresponds to remove coordinated and adsorbed water. The other stage starts from 289ºC to 375ºC ($T_{max=}$ 334ºC), corresponds to dehydroxylation of kaolin[1,7,11].

TGA and DTA curves for group B (Fig. 9) show that UK-AP has two stages of decomposition. The first stage is in the range from 135ºC to 282ºC ($T_{max=}$ 203ºC), the second stage in the range from 339ºC to 609ºC ($T_{max=}$ 506ºC). Coating of UK-AP by urea-formaldehyde (UF) polymer increases the decomposition stages to three stages for UK-AP-UF. First stage is in the range from 164ºC to 316ºC ($T_{max=}$ 243ºC), second stage is in the range from 380ºC to 586ºC ($T_{max=}$ 507ºC) and the third stage is in the range from 586ºC to 667ºC ($T_{max=}$ 626ºC).

TGA and DTA curves for group C (Fig. 10) indicate that UK-UF has two decomposition stages. First stage is in the range from 146ºC to 333ºC ($T_{max=}$ 280ºC) and second stage is in the range from 351ºC to 592ºC ($T_{max=}$ 517ºC). UK-UF-AP show also two stages, first stage is in the range from 170ºC to 325ºC ($T_{max=}$ 263ºC) and second stage is in the range from 413ºC to 556ºC ($T_{max=}$ 485ºC).

These previous results obviously show that dry grinding of urea with kaolin for intercalation causes decreasing in thermal stability for kaolin (**K** $T_{max=}$ 535ºC/ **UK** $T_{max=}$ 334ºC). This is because of amorphization or the distortion of kaolin structural morphology. Also, mechanochemical dehydroxylation resulted in increasing the amount of adsorbed/co-ordinated water[1,7].

Treatment of UK with APTES silane coupling agent increases thermal stability (**UK** $T_{max=}$ 334ºC/ **UK-AP** $T_{max=}$ 506ºC). This is due to presence of amino ends groups at APTES helps in successful grafting on edges, surface and inside kaolin layers[9].

Coating of UK-AP by UF polymer increases thermal stability (**UK** $T_{max=}$ 334ºC/ **UK-AP-UF** $T_{max=}$ 626ºC). Thermal stability for UK-AP-UF resulted from presences of UK-AP which has better compatibility with UF polymer. Also, the network of crosslinked UF polymer around UK-AP can prevent molecules from releasing and escaping[8].

Encapsulating of UK by UF polymer increases thermal stability compared with UK (**UK** $T_{max=}$ 334ºC/ **UK-UF** $T_{max=}$ 517ºC). This is due to presence of active groups inside kaolin layers enables UF polymer for constructions of crosslinked network that improving thermal stability for UK-UF. Grafting of APTES silane coupling agent molecules on the surface of UK-UF also, increases thermal stability compared with UK due to the presence of large molecules of APTES with its functional groups above the crosslinked polymer[8,9].

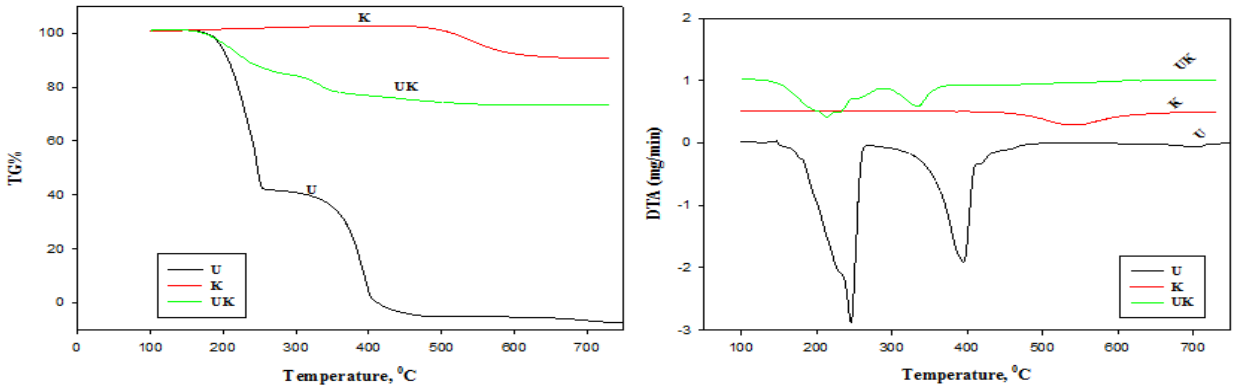


**Fig. 8:** TGA and DTA curves of group A **(U, K and UK)**

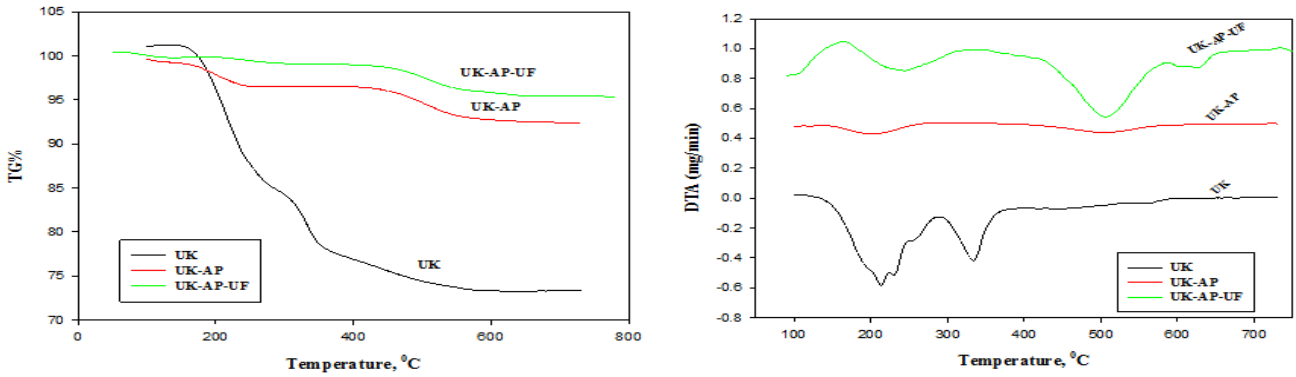


**Fig. 9:** TGA and DTA curves of group B **(UK, UK-AP and UK-AP-UF)**

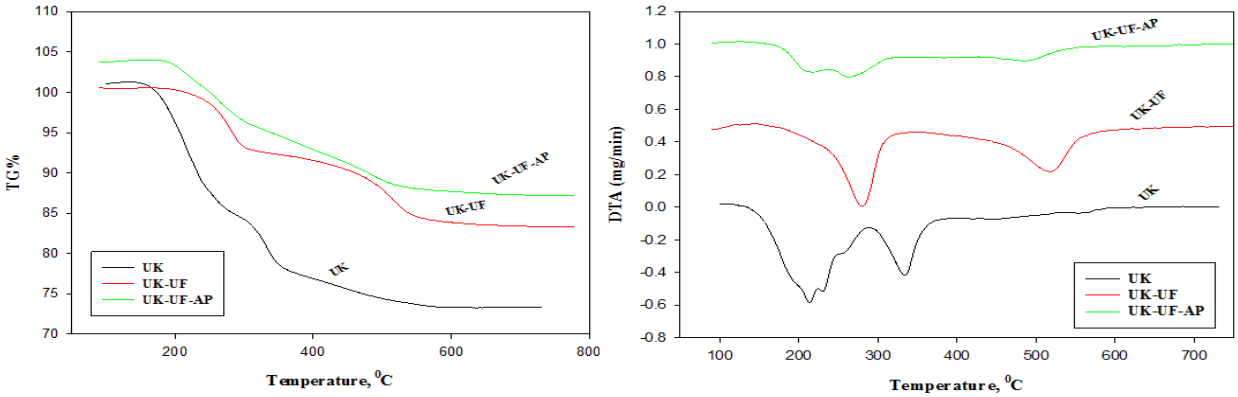


**Fig. 10:** TGA and DTA curves of group C **(UK, UK-UF and UK-UF-AP)**

**Table (2): Temperature of Different Decomposition Rates for Prepared Samples**

| Specimens | T Initial (°C) | T Final (°C) | T Max (°C) |
|---|---|---|---|
| **U** | | | |
| **1st peak** | 217 | 259 | 246 |
| **2nd peak** | 355 | 410 | 395 |
| **K** | | | |
| **1st peak** | 469 | 619 | 535 |
| **UK** | | | |
| **1st peak** | 153 | 253 | 213 |
| **2nd peak** | 301 | 354 | 334 |
| **UK-AP** | | | |
| **1st peak** | 148 | 261 | 203 |
| **2nd peak** | 415 | 574 | 506 |
| **UK-AP-UF** | | | |
| **1st peak** | 175 | 310 | 243 |
| **2nd peak** | 440 | 565 | 507 |
| **3rd peak** | 589 | 645 | 626 |
| **UK-UF** | | | |
| **1st peak** | 236 | 307 | 280 |
| **2nd peak** | 451 | 556 | 517 |
| **UK-UF-AP** | | | |
| **1st peak** | 180 | 311 | 263 |
| **2nd peak** | 438 | 523 | 485 |

### 2.3.4. Energy Dispersive X-ray Analysis (EDX)

Elemental analysis of prepared samples resulting from the EDX analysis technique is presented in table (3) and Figs. (11, 12 and 13). EDX results show the basic elements (C, O, Si and Al) present in all prepared samples [42] but, (N) present in all samples by a noticeable weight percentage except K. This observation confirms the success of the treatment of K and the beneficial preparation of all powder samples.

**Table 3. EDX analysis of prepared samples**

| Elements | C | O | Si | Al | N | Mg | Fe | Ca | K | Ti |
|---|---|---|---|---|---|---|---|---|---|---|
| **K** (Weight%) | 16.95 | 48.89 | 16.09 | 16.65 | ---- | 0.02 | 0.63 | 0.01 | 0.69 | **0.08** |
| **UK** (Weight %) | 14.34 | 43.08 | 16.31 | 14.96 | ***10.02*** | 0.01 | 0.44 | 0.05 | 0.63 | **0.15** |
| **UK-AP** (Weight %) | 12.55 | 51.14 | 21.76 | 9.64 | ***2.14*** | 0.18 | 1.12 | 0.11 | 1.02 | **0.35** |
| **UK-AP-UF** (Weight %) | 12.41 | 50.12 | 25.72 | 8.92 | ***1*** | ---- | 0.77 | 0.2 | 0.55 | **0.31** |
| **UK-UF** (Weight %) | 10.51 | 52.83 | 15.68 | 15.27 | ***3.33*** | 0.35 | 0.79 | 0.06 | 1.06 | **0.12** |
| **UK-UF-AP** (Weight %) | 32.43 | 39.82 | 13.36 | 10.21 | ***2.45*** | ---- | 0.81 | 0.14 | 0.62 | **0.16** |

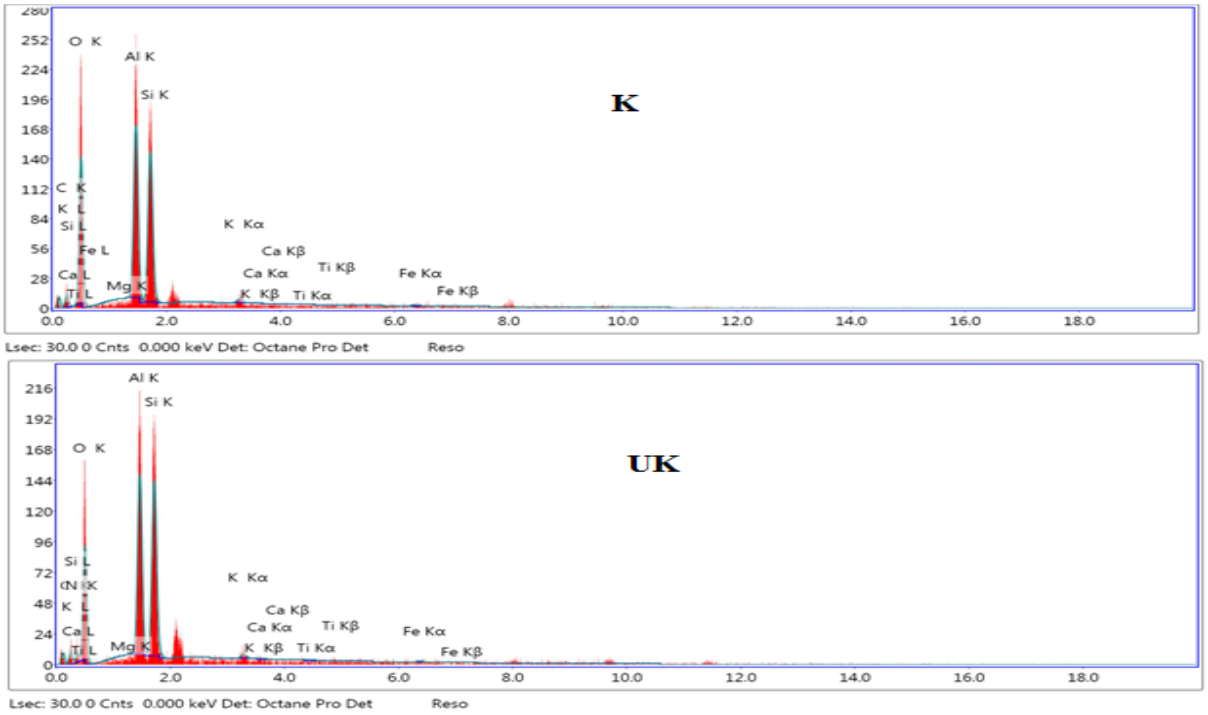


**Fig. 11:** EDX spectra of **K** and **UK**

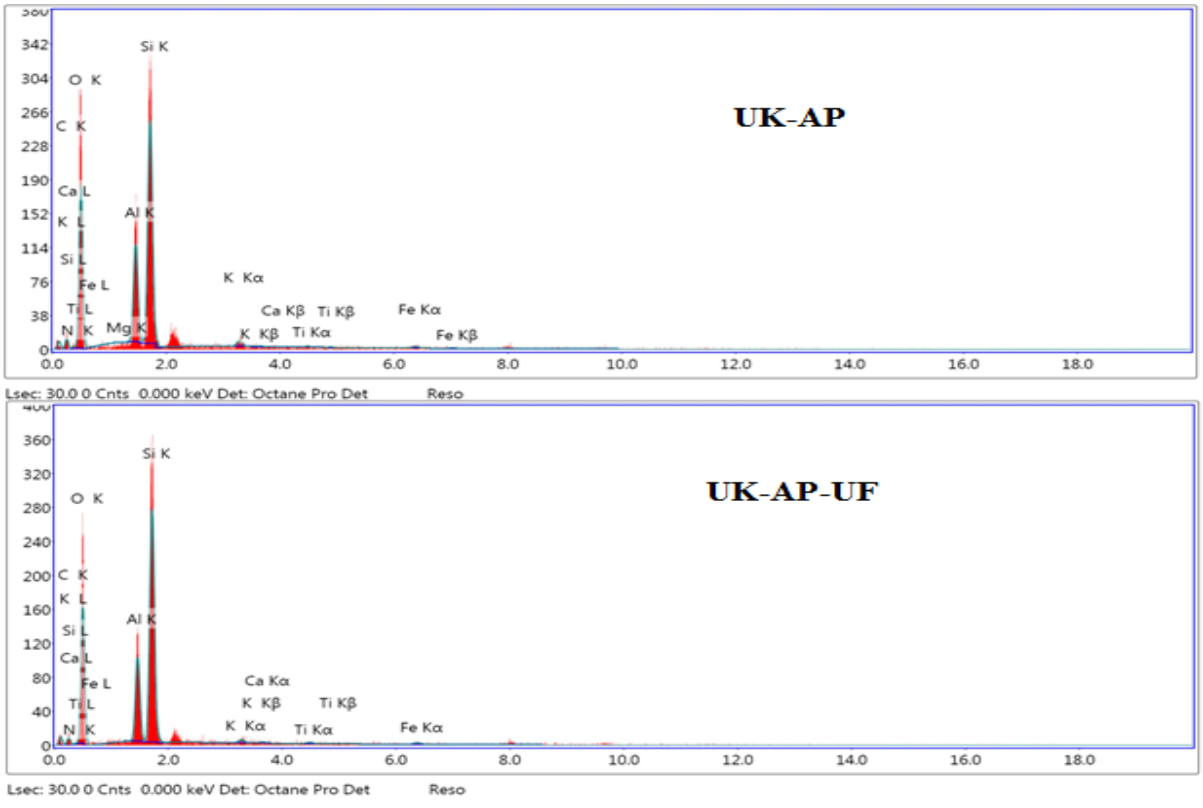


**Fig. 12:** EDX spectra of **UK-AP** and **UK-AP-UF**

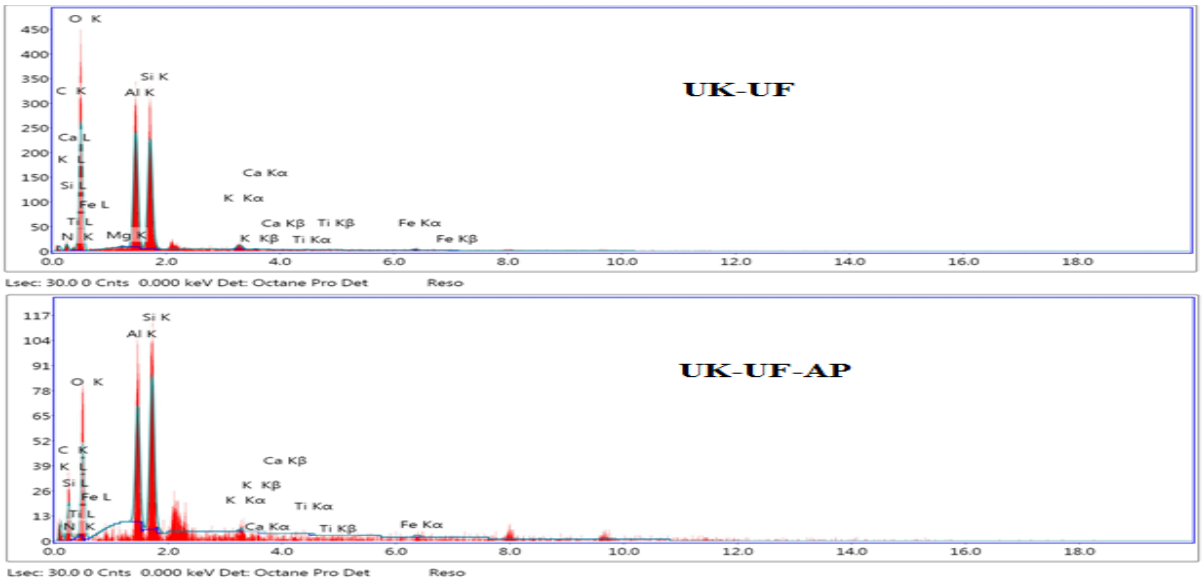


**Fig. 13:** EDX spectra of **UK-UF** and **UK-UF-AP**

### 2.3.4. Scanning Electron Microscopy (SEM)

Morphological variations of all prepared samples were studied by SEM images and illustrated in Fig. (14). Fig. 14A clearly indicates the kaolin's platelets with a sharp, irregular shape up to a diameter of 4µm[4,7,8,10,38]. Dry grinding of the urea molecules with kaolin causes cracks in the layers or platelets of kaolin to a smaller size than original kaolin, as indicated in Fig. (14B)[7]. After treatment of UK with APTES silane coupling agent, small spherical and spheroid particles of organic silanes appear on the SEM picture in Fig. (14C) indicating the success of grafting of silanes[24]. Picture of the UK-AP-UF shows that the small particles of organic silanes and whole particles were coated by a thin film of urea-formaldehyde polymer, forming a shell (Fig. 14D)[8,10,13].

As for the picture of UK-UF, it shows that the sharp edges of kaolin's layers convert to smooth ones, which is a confirmation of the surrounding of urea-formaldehyde polymer around treated kaolin Fig. (14E)[8]. The same observation is dedicated in the UK-UF-AP SEM picture in the same diameter but with more noticeable small particles of organic silane and with more surrounding by polymer shellFig. (14F)[8,10].

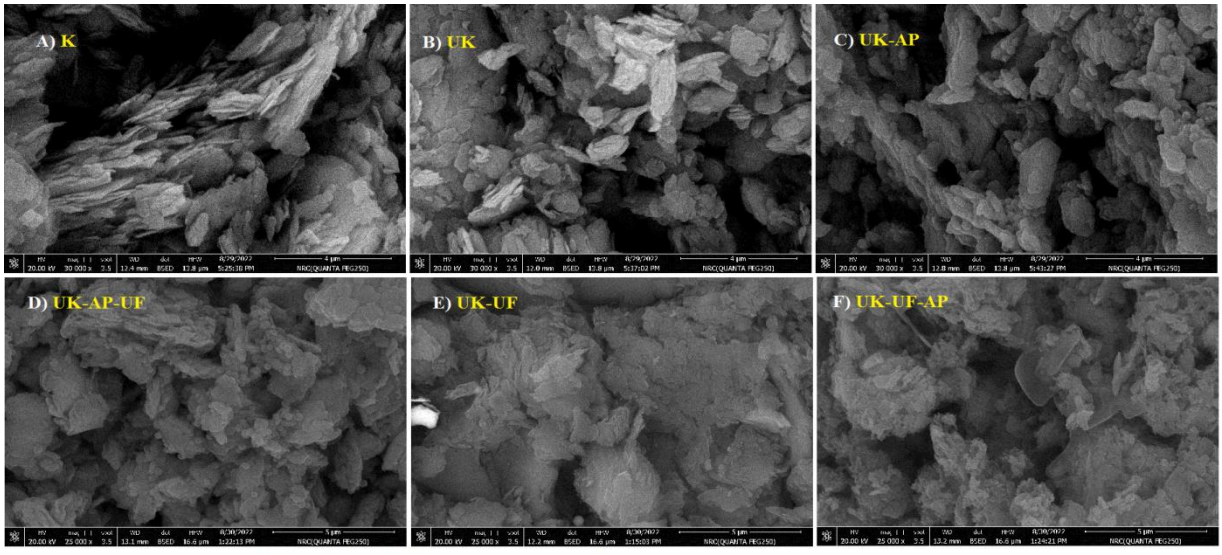


**Fig. 14:** SEM pictures of all prepared samples

### 2.3.5. Visual immersion corrosion test

The visual immersion corrosion test is a qualitative test to investigate the performance of the prepared fillers via recording the rust and blisters degree. The coated steel panels immersed in 3.5% NaCl solution for 28 days that were coated by the prepared varnish formulations presented in Fig. 15. **F1** (alkyd resin as blank) shows a high degree of rusting and some blisters. **F2**

(alkyd resin with ZP pigment as blank)exhibits a less degree of rust and blister**.** Zinc phosphate added to alkyd resin slows the corrosion degree and inhibits the corrosive anodic reaction[26-29].**F3** (alkyd resin with K)also shows less degree of rust and blisters due to the platy shape, crystal structure, surface chemistry and fine particle size of kaolin[3,7].**F4** (alkyd resin with UK) indicated a high degree of rust with less blistering due to the partial deformation of the kaolin crystal structure[1,7].**F5** (alkyd resin with UK-AP) showed less rust and blisters than F1, F3 and F4 because of the grafting of APTES on the surface of UK and in between its layers, which made the kaolin the finest in particle size[5,9,10].**F6, F7** and **F8** (alkyd resin with UK-AP-UF, UK-UF and UK-UF-AP, respectively) exhibited the lowest degree of rust and blisters. This is evidence that the encapsulated fillers have superior anticorrosive properties and protect the mild steel from corrosion similar to ZP [8, 13, 14, 43]. Table (4) indicates the rust and blister degree after 28 days of immersion in 3.5% NaCl solution.

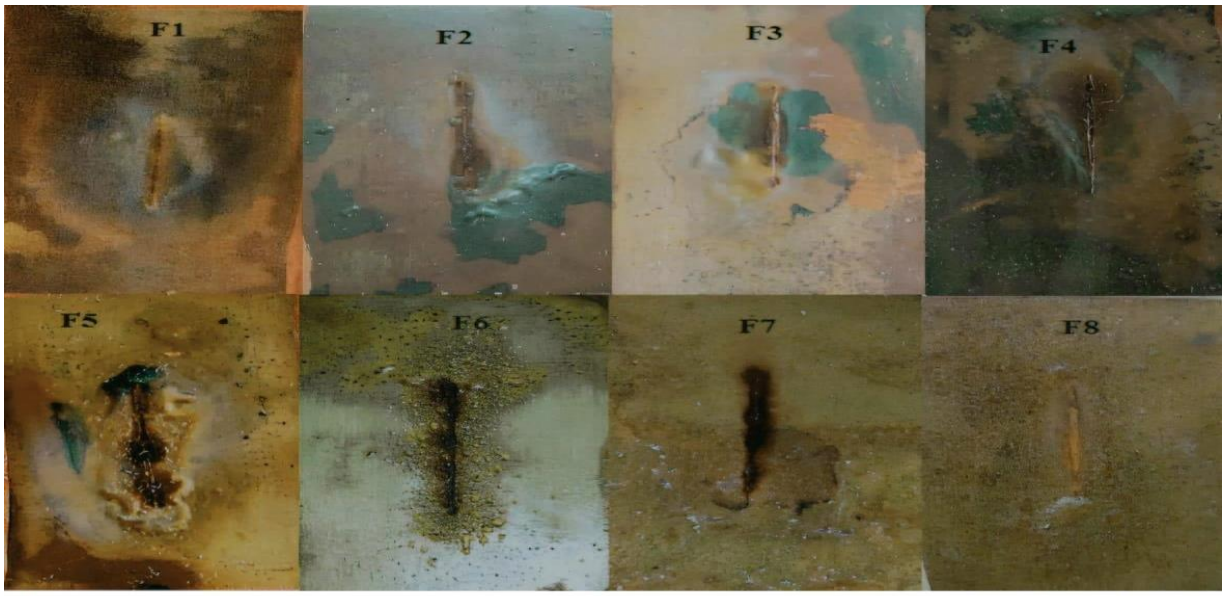


**Fig. 15:** Corrosion test photos of coated steel panels after immersion for 28 days in 3.5% NaCl solution

Table (4): Rust and Blisters degree of varnish formulations after immersion for 28 days in 3.5% NaCl solution.

| *Formula No.* | *Degree of rust (DR)* | ***Degree of blister (DB)*** |
|---|---|---|
| **F1** | 4G | **7M** |
| **F2** | 9S | **9F** |
| **F3** | 5S | **9F** |
| **F4** | 3G | **8F** |
| **F5** | 8S | **9F** |
| **F6** | 9S | **9M** |
| **F7** | 9S | **9F** |
| **F8** | 9S | **9F** |

(S) Spot rusting, (G) General rusting, (M) Medium and (F) Few.

***2.3.6. Electrochemical Impedance Spectroscopy (EIS)***

According to preliminary reliable corrosion resistance of coated steel panels immersed in 3.5% NaCl solution for 28 days (at visual immersion corrosion test), the immersion time was extended to 40 days in the EIS study. EIS measurement is a non-destructive and quantitative method for estimating the anticorrosive varnish coating performance[44]. Increasing solution penetration through the varnish coating by extending the immersion time leads in general to corrosive damage or crack points on the coat/steel substrate surface[45]. Illustration ofthe role of the prepared new active fillers in repairing the corrosive damage points was indicated in data recorded from the electrical equivalent circuits fitting (Fig. 16) of Nyquist plots (Fig. 17, Fig. 18 and Fig. 19) at table (5). The fitted parameters are **Rs** is the 3.5% NaCl solution resistance, **Rc** is the formulated varnish coating resistance (indication for porosity of coating and its barrier effect), **Cc** is the capacitance of coating (quantitative indication for the coating water uptake), **Rct** is the charge transfer resistance (indication for the value of anticorrosive protection of the substrate), **Cdl** is the capacitance of the double layer (indication for the delamination of varnish coating), and **Zw** is Warburg impedance (simulation ofthe mass-transport effect)[46, 47].

Figs. 17, 18 and 19 show the Nyquist plots for steel blanks, with the suitable equivalent circuit model for each recorded plot. The plots wererecorded after 3, 20 and 40 days of immersion in 3.5% NaCl solution. In Fig. 17, the mild steel was in direct contact with corrosive ions in the solution during the soaking time, so it exhibits the lowest coating resistance (Rc range from

0.22 to 0.44 Ω.cm$^2$). F1 (alkyd resin as blank1) shows Rc 14.5Ω.cm$^2$ and decreases to 6.6Ω.cm$^2$ after 40 days of immersion. Furthermore, F1 shows Rct 5.32Ω.cm$^2$ and increases to 13Ω.cm$^2$ after 40 days. After adding ZP as a known anticorrosive pigment to alkyd resin (F2 alkyd resin with ZP as blank2), Rc and Rct values after 20 days of immersion equal 46.5 and 59.7Ω.cm$^2$ respectively, and then decrease to 39.6 and 19Ω.cm$^2$ after 40 days of immersion, respectively. Through EIS results of the three blanks (steel, F1and F2), alkyd resin provides a protective varnish coat to prevent steel from direct connection with undesirable ions in solution. Butthe addition of ZP to alkyd resin enhanced the inhibition of penetration of corrosive ions inside the coat interface[26-29].

In Fig. 18, the Rc value for F3 (alkyd resin with K) equals 40.6Ω.cm$^2$ after 3 days of immersion and decreases to 21.4Ω.cm$^2$ after 40 days of immersion. Likewise, Rct value equals 53.5Ω.cm$^2$ after 3 days and then decreases to 10.3Ω.cm$^2$ after 40 days[46-48]. As for F4 (alkyd resin with UK), the Rc value increases from 8.62Ω.cm$^2$ (after 3 days) to 27.8Ω.cm$^2$ (after 40days), but the Rct value decreases to 16.1Ω.cm$^2$ after 20days of immersion. F5 (alkyd resin with UK-AP): Rc value decreases from 30.8Ω.cm$^2$ (after 3 days) to 7.04Ω.cm$^2$ (after 40 days) and Rct decreases from 38.8 Ω.cm$^2$ (after 3 days) to 8.78 Ω.cm$^2$ (after 40 days). Decreasing varnish coating resistance (Rc) value and charge transfer resistance (Rct) resulted from increasing the days of immersion. Comparing the effect of K, UK and UK-AP with ZP pigment, the three fillers exhibit the required decreasing of penetration of corrosive ions[51].

In Fig. 19, F6 (alkyd resin with UK-AP-UF) has Rc and Rct values of 27.7Ω.cm$^2$ and 28.2 Ω.cm$^2$, respectively (after 3 days), that decrease to 11Ω.cm$^2$ and 15.2 Ω.cm$^2$ (after 40 days). Also, the values of Rc and Rct for F7 (alkyd resin with UK-UF) decrease from 32.1Ω.cm$^2$ and 50 Ω.cm$^2$, respectively (after 3 days) to 11.2Ω.cm$^2$ and 7.36 Ω.cm$^2$ (after 40 days). F8 (alkyd resin with UK-UF-AP) exceeded expectations, as Rc and Rct values after 3 days of immersion equaled 13×10$^3$Ω.cm$^2$ and 7.36×10$^3$Ω.cm$^2$ respectively, but after a long time of immersion the Rc and Rct values decreased due to the penetration of corrosive ions into the steel substrate. Comparing the three encapsulated fillers with ZP pigment, the performance of F6 and F7 is nearly the same as the modified kaolin coated with a shell of urea-formaldehyde polymer (UF). F8 has superior anticorrosive properties to protect steel in corrosive mediums[51-55].

Data and results of EIS measurements showed that these new active fillers can be used as anticorrosive fillers, especially UK-UF-AP. The encapsulated filler UK-UF-AP has two layers, a layer of UF polymer covered with a layer of APTES (silane coupling agent). This causes better adhesion of the varnish coating to the mild steel substrate surface due to the presence of Si bonds and $N_2$ atoms in APTES and UF polymer. The APTES layer hinders corrosive ions' movement through the varnish coating interface and develops the barrier properties of the coating.

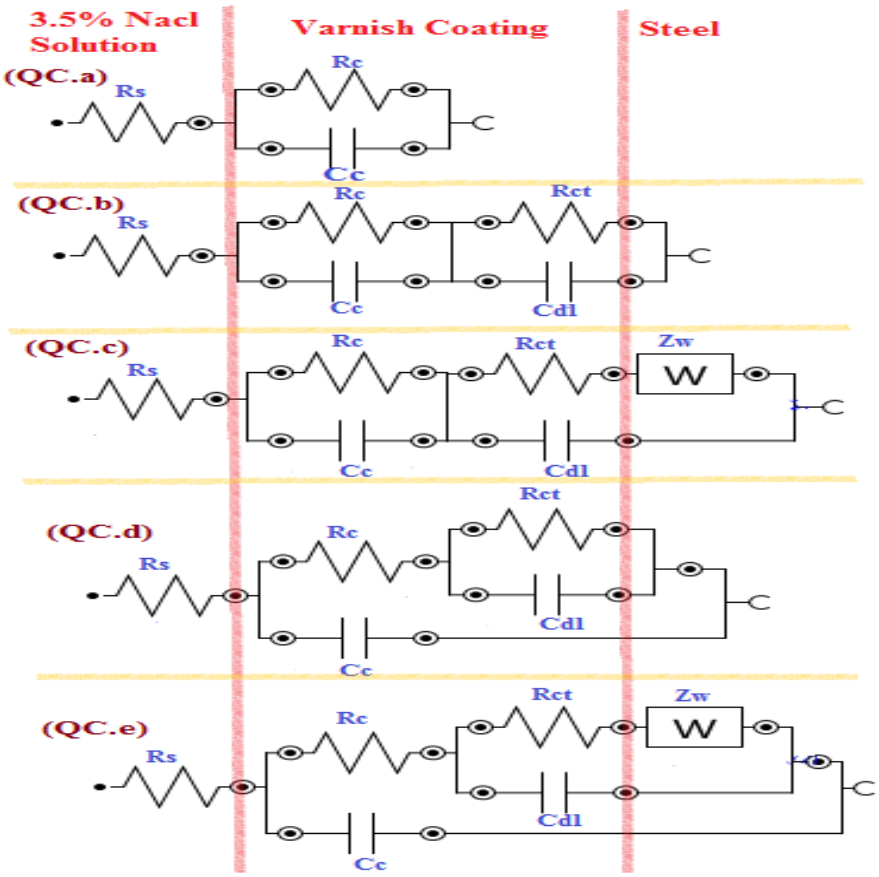


**Fig. 16**: Equivalent circuits used to simulate the varnish formulations coating/mild steel system

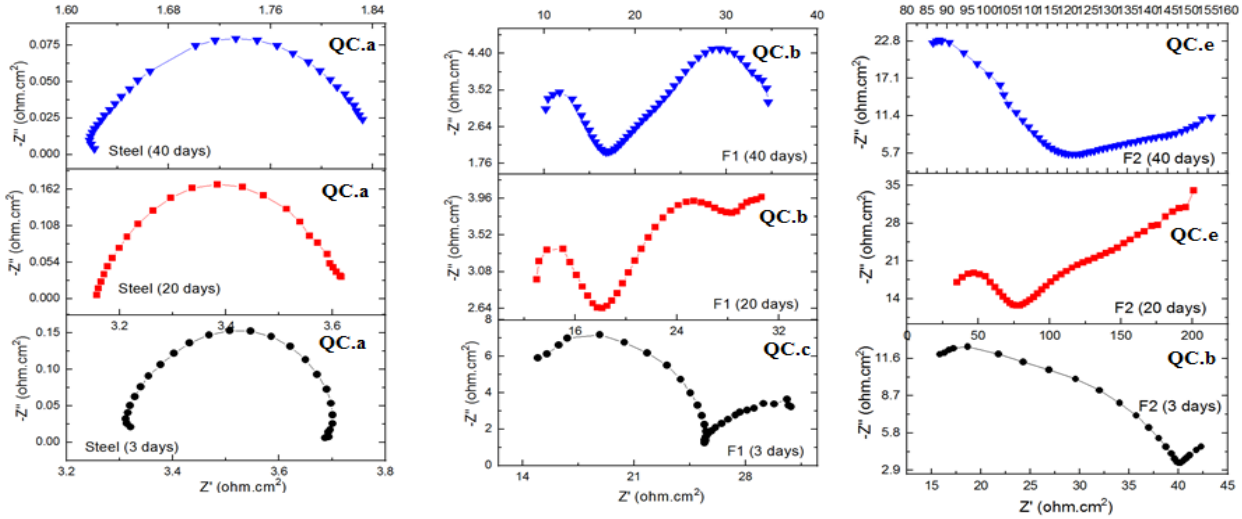


**Fig. 17 :** EIS Nyquist plots of steel blank, F1and F2 immersed in 3.5% NaCl solution

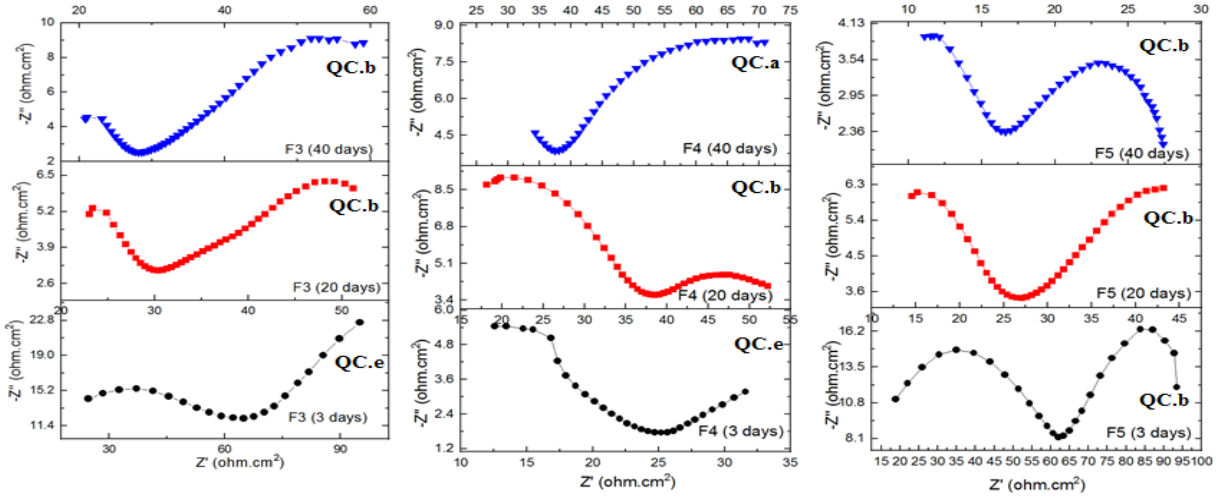


**Fig. 18:** EIS Nyquist plots of F3, F4 and F5 immersed in 3.5% NaCl solution

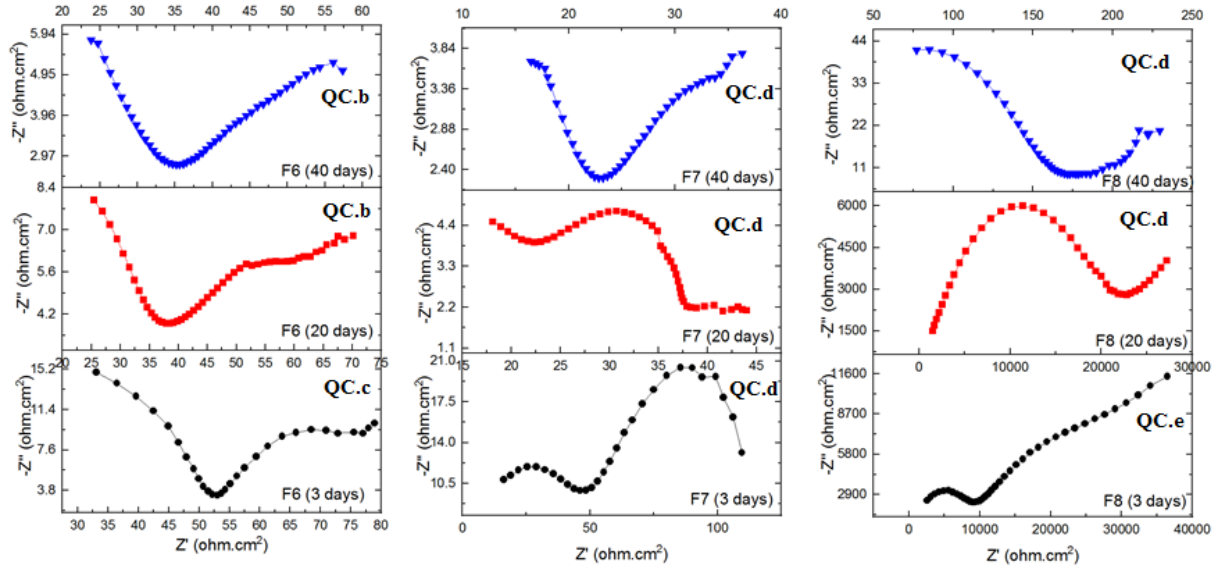


**Fig. 19 :** EIS Nyquist plots of F6, F7 and F8 immersed in 3.5% NaCl solution

**Table (5): The fitted data of EIS equivalent circuits**

| Sample | Time/day | Rs (Ω.cm²) | Rc(Ω.cm²) | C c | Rct (Ω.cm²) | C ct | Zw[mMho*sˆ(1/2)] |
|---|---|---|---|---|---|---|---|
| **Steel** | 3 | 3.35 | 0.33 | 985 µF | …… | ….. | …… |
| | 20 | 3.19 | 0.40 | 4.51 mF | …… | ….. | …… |
| | 40 | 1.61 | 0.22 | 6.30 mF | …… | ….. | …… |
| **F1** | 3 | 11 | 14.5 | 154 nF | 5.32 | 1.77 mF | 92.7 |
| | 20 | 13.9 | 6.59 | 3.03 µF | 10.1 | 170 µF | …… |
| | 40 | 13 | 6.62 | 5.97 µF | 13 | 1.38 mF | …… |
| **F2** | 3 | 16.8 | 23.6 | 154 nF | 18.7 | 486 µF | …… |
| | 20 | 34 | 46.5 | 440 nF | 59.7 | 45.3 µF | 12.1 |
| | 40 | 75.8 | 39.6 | 224 nF | 19 | 130 µF | 45.4 |
| **F3** | 3 | 23.9 | 40.6 | 162 nF | 53.5 | 16.1 µF | 35.7 |
| | 20 | 27.1 | 10 | 13.4 µF | 16.8 | 1.61 mF | ….. |
| | 40 | 25.5 | 21.4 | 3.55 mF | 10.3 | 31.3 µF | ….. |
| **F4** | 3 | 16.5 | 8.62 | 963 nF | 11.8 | 304 µF | 105 |
| | 20 | 18.9 | 18.4 | 809 nF | 16.1 | 459 µF | …… |
| | 40 | 35.4 | 27.8 | 465 µF | …… | …… | …… |
| **F5** | 3 | 18.9 | 30.8 | 30.3 µF | 38.8 | 185 nF | …… |
| | 20 | 16.6 | 12.2 | 1.88 µF | 18.5 | 588 µF | …… |
| | 40 | 10.5 | 7.04 | 1.73 µF | 8.78 | 182 µF | …… |
| **F6** | 3 | 25.2 | 27.7 | 104 nF | 28.2 | 64.5 µF | 29.9 |
| | 20 | 24.8 | 15.2 | 1.37 µF | 21 | 543 µF | …… |
| | 40 | 25.4 | 11 | 3.37 µF | 15.2 | 1.49 mF | …… |
| **F7** | 3 | 16.1 | 32.1 | 225 nF | 50 | 19.2 µF | …… |
| | 20 | 17.8 | 9.53 | 2.51 µF | 12.1 | 90.3 µF | …… |
| | 40 | 18.5 | 11.2 | 836 µF | 7.36 | 6.10 µF | …… |
| **F8** | 3 | 2.19 ˣ$10^3$ | 13 ˣ$10^3$ | 380 nF | 7.36ˣ$10^3$ | 2.68 nF | 23.6 |
| | 20 | 1.39 ˣ$10^3$ | 13.5 ˣ$10^3$ | 32.2 nF | 5.64ˣ$10^3$ | 5.64 nF | …… |
| | 40 | 68 | 90.9 | 180 nF | 57.8 | 243 µF | …… |

## Conclusion

In this paper**,** we advanced new active anticorrosive fillers which were used to protect steel surfaces from corrosion. By mechanical dry grinding, kaolin was intercalated by urea to partially separate the ordered layers of kaolin and generate broken bonds. These broken bonds served as new sites of functional groups capable of grafting of silane molecules or polymer chains inside and outside its surface. The intercalation of kaolin was followed by grafting silane coupling agent then encapsulated by a shell of urea-formaldehyde polymer layer. FTIR spectroscopy, X-ray diffraction, SEM and thermal analysis data confirmed the intercalation of urea molecules throughout the kaolin layers causing partial breaking down in the crystal structure. The results also proved the grafting of silane and polymer chains inside layers and outside surface, which accompanied by increasing thermal stability as it was emphasized by shifting of DTA peaks to higher temperatures. SEM studies confirmed the polymer chains surrounded kaolin particles were forming a continuous shell encapsulation. SEM micrographs showed also the dry grinding of kaolin-urea mixture was producing sharpless and compact aggregates of nanometer-sized kaolin spheroids. The EDX studies proved the existence of active N and Si bonds on the filler surface which can be useful in application as anticorrosive fillers for mild steel protection. EIS study indicated the anticorrosive properties of the prepared fillers especially the encapsulated filler UK-UF-AP, as Rc and Rct values equaled $13^{\times}10^3\Omega.cm^2$ and $7.36^{\times}10^3\Omega.cm^2$, respectively. The proved efficiency of these fillers gives the opportunity to complete future electrochemical study on a progressed paper soon.

## Conflicts of interest

The authors have no conflict of interest.

## Acknowledgments

This work was financially supported by the Doctoral Program of National Research Centre, Dokki, Egypt.

## References

1. Zhang, S., et al., Mechanism associated with kaolinite intercalation with urea: Combination of infrared spectroscopy and molecular dynamics simulation studies. The Journal of Physical Chemistry C,121(1): (2017) p. 402-409.
2. Bergaya, F. and G. Lagaly, Handbook of clay science. (2013): Newnes.
3. Buyondo, K.A., H. Kasedde, and J.B. Kirabira, A comprehensive review on kaolin as pigment for paint and coating: Recent trends of chemical-based paints, their environmental impacts and regulation. Case Studies in Chemical and Environmental Engineering,6 (2022) p. 100244.

4. Chi, Q., et al., The role of exfoliated kaolinite on crystallinity, ion conductivity, thermal and mechanical properties of poly (ethylene oxide)/kaolinite composites. Polymer Bulletin, 74 (2017) p. 3089-3108.
5. Zhang, S., et al., Intercalation of γ-aminopropyl triethoxysilane (APTES) into kaolinite interlayer with methanol-grafted kaolinite as intermediate. Applied Clay Science, 114 (2015) p. 484-490.
6. Ibrahim, W.M.A.W., et al., Alkaline-Activation Technique to Produce Low-Temperature Sintering Activated-HAp Ceramic. Applied Sciences, 13(4): (2023) p. 2643.
7. Makó, É., et al., Kaolinite–urea complexes obtained by mechanochemical and aqueous suspension techniques—a comparative study. Journal of Colloid and Interface Science, 330(2): (2009) p. 367-373.
8. Chen, S., et al., Preparation and characterization of urea-formaldehyde resin/reactive kaolinite composites. Particuology, 24 (2016) p. 203-209.
9. Yang, S.-q., et al., Effect of reaction temperature on grafting of γ-aminopropyl triethoxysilane (APTES) onto kaolinite. Applied clay science, 62 (2012) p. 8-14.
10. Tao, Q., et al., Silylation of mechanically ground kaolinite. Clay minerals, 49(4): (2014) p. 559-568.
11. Seifi, S., et al., Kaolin intercalated by urea. Ceramic applications. Construction and Building Materials, 113 (2016) p. 579-585.
12. Mahdavi, F., R.S. Abdul, and Y.M. Khanif, Intercalation of urea into kaolinite for preparation of controlled release fertilizer. Chemical Industry and Chemical Engineering Quarterly, 20(2): (2014) p. 207-213.
13. Rochmadi, A.P. and W. Hasokowati, Mechanism of microencapsulation with urea-formaldehyde polymer. Am. J. Appl. Sci, **7**(6): (2010) p. 739-745.
14. Li, W., et al., Preparation and properties of melamine urea-formaldehyde microcapsules for self-healing of cementitious materials. Materials, 9(3): (2016) p. 152.
15. Khorramabadi, L.A., R. Behrooz, and S. Kazemi, Effects of nanoclay modification with aminopropyltriethoxysilane (APTES) on the performance of urea–formaldehyde resin adhesives. BioResources, 18(3): (2023) p. 5417.
16. Li, J. and Y. Zhang, Morphology and crystallinity of urea-formaldehyde resin adhesives with different molar ratios. Polymers, 13(5): (2021) p. 673.
17. Nguon, O., et al., Microencapsulation by in situ polymerization of amino resins. Polymer reviews, 58(2): (2018) p. 326-375.
18. Baharin, N.K., et al., Hirshfeld, Surface Analysis, Density Functional theory and Corrosion Inhibition Mechanism Proposed of Vanillin 4-ethylthiosemicarbazone on the Mild Steel in 1M HCl. Moroccan Journal of Chemistry, 13(1): (2025) p. 80-105.
19. Belkheiri, A., et al., Evaluation of 14-(p-tolyl)-14H-dibenzo [a, j] xanthene as a highly efficient organic corrosion inhibitor for mild steel in 1 M HCl: Electrochemical, theoretical, and surface characterization. International Journal of Electrochemical Science, 19(12): (2024) p. 100873.
20. Wang, Q., et al., Development of pH-sensitive chitosan/plant extract microcapsules: Enhanced corrosion protection for carbon steel in HCl solution. International Journal of Biological Macromolecules, 282 (2024) p. 137461.
21. Sehrawat, R., et al., Synergistic corrosion inhibition of mild steel by chalcone derivatives and KI in acidic media via computational and experimental methods. Progress in Organic Coatings, 198: (2025) p. 108911.
22. Gab-Allah, M.G., A.H. Elged, and M.F. Bakr, Empirical and Computational Investigation of Cationic Gemini Surfactants as Anti-Corrosive Inhibitors for Mild Steel in Acid Medium and its silver Nano Structure synthesis and Analysis. Egyptian Journal of Chemistry, 66(13): (2023) p. 2013-2031.
23. Fouda, A.E., et al., Inhibition efficiency of erdosteine drug for 304L stainless steel corrosion and its solvation thermodynamic parameters. Egyptian Journal of Chemistry, 65(132): (2022) p. 455-475.
24. Liu, X., et al., A route for large-scale preparation of multifunctional superhydrophobic coating with electrochemically-modified kaolin for efficient corrosion protection of magnesium alloys. Journal of Magnesium and Alloys, 10(11): (2022) p. 3082-3099.
25. Li, Z., et al., Urea-formaldehyde resin covered etched basalt as durable composite coating with antibacterial activity and corrosion resistance. Corrosion Science,209 (2022) p. 110760.
26. Xue, Y.-N., et al., Mass preparation and anticorrosion mechanism of highly triple-effective corrosion inhibition performance for co-modified zinc phosphate-based pigments. Dyes and Pigments, 161 (2019) p. 489-499.
27. Hao, Y., et al., The mechanism of inhibition by zinc phosphate in an epoxy coating. Corrosion Science, 69 (2013) p. 77-86.
28. Yang, S., et al., A comparative study on the anti-corrosive performance of zinc phosphate in powder coatings. Coatings, 12(2): (2022) p. 217.

29. Tian, J.-J., et al., Zinc Phosphate/Imidazole Composites Built on Coordinating Construction for the Syncretic Weatherability and Corrosion Inhibition Property. Industrial & Engineering Chemistry Research, 63(40): (2024) p. 17207-17220.
30. Aroke, U., U. El-Nafaty, and O. Osha, Properties and characterization of kaolin clay from Alkaleri, North-Eastern Nigeria. International Journal of Emerging Technology and Advanced Engineering, 3(11): (2013) p. 387-392.
31. Yan, H., W. Yuanhao, and Y. Hongxing, TEOS/silane-coupling agent composed double layers structure: a novel super-hydrophilic surface. Energy Procedia, 75 (2015) p. 349-354.
32. ASTM D 1210-05 (2022) Standard Test Method for Fineness of Dispersion of Pigment-Vehicle Systems by Hegman-Type Gage 1.
33. Diab, W.W., et al., Promoting the effect of zinc-rich epoxy via poly (aniline-co-anisidine)/iron waste composite on corrosion protection of steel. Polymer Composites,40(12): (2019) p. 4682-4693.
34. ASTM D610-08 (2019) Standard Practice for Evaluating Degree of Rusting on Painted Steel Surfaces.
35. ASTM D714-02 (2017) Standard Test Method for Evaluating Degree of Blistering of Paints.
36. El-Moaz, Y.A., et al., Fabrication, Characterization, and Corrosion Protection of Siloxane Coating on an Oxygen Plasma Pre-treated Silver-Copper Alloy. Journal of Materials Engineering and Performance, 32(19): (2023) p. 8818-8830.
37. Tironi, A., et al., Thermal treatment of kaolin: effect on the pozzolanic activity. Procedia Materials Science, 1 (2012) p. 343-350.
38. Gan, C., et al., Characterization and hemostatic potential of two kaolins from southern China. Molecules,24(17): (2019) p. 3160.
39. Grdadolnik, J. and Y. Maréchal, Urea and urea–water solutions—an infrared study. Journal of Molecular Structure, 615(1-3): (2002) p. 177-189.
40. Shahariar, G.H. and O.T. Lim, A study on urea-water solution spray-wall impingement process and solid deposit formation in urea-SCR de-NOx system. Energies, 12(1): (2018) p. 125.
41. Zhu, N., et al., Thermogravimetric experiment of urea at constant temperatures. Materials, 14(20): (2021) p. 6190.
42. Sabbagh, F., et al., Mechanical properties and swelling behavior of acrylamide hydrogels using montmorillonite and kaolinite as clays. J. Environ. Treat. Tech, **7**(2): (2019) p. 211-219.
43. Xie, B., et al., Self-healing polyurethane anticorrosive coatings based on alkyd resin microcapsules. Materials and Corrosion,75(9): (2024) p. 1090-1099.
44. Nazari, M.H., et al., Nanocomposite organic coatings for corrosion protection of metals: A review of recent advances. Progress in Organic Coatings, 162 (2022) p. 106573.
45. Bagale, U.D., et al., Green synthesis of nanocapsules for self-healing anticorrosion coating using ultrasound-assisted approach. Green Processing and Synthesis, **7**(2): (2018) p. 147-159.
46. Cano, E. and B. Ramírez Barat, Electrochemical techniques for in situ corrosion evaluation of cultural heritage. Advanced characterization techniques, diagnostic tools and evaluation methods in heritage science, (2018) p. 21-32.
47. Macdonald, J.R., Impedance spectroscopy. Annals of biomedical engineering, 20 (1992) p. 289-305.
48. Sheng, P., D. Wang, and G. Yu, Effect of Kaolin Addition on Electrochemical Corrosion Resistance of Duplex 2205 Stainless Steel Embedded in Concrete Exposed in Marine Environment. International Journal of Electrochemical Science, 15(12): (2020) p. 11732-11741.
49. Baghdad, M. and B. Ait Saadi, Electrochemical and characterisation study of corrosion of reinforcing steel embedded in kaolinite: two-year exposure study. Corrosion Engineering, Science and Technology, 56(1): (2021) p. 35-49.
50. Zhang, Y., et al., Characterization of Nano-kaolin and its enhancement of the mechanical and corrosion resistance of epoxy coatings. Materials Today Communications,41 (2024) p. 110371.
51. Xavier, J.R., Investigation into the effects of silanized nanoclay on the barrier properties of epoxy resin in chloride environment. Journal of Molecular Structure, 1264 (2022) p. 133264.
52. Zhou, X., et al., Smart corrosion inhibitors for controlled release: a review. Corrosion Engineering, Science and Technology, 58(2): (2023) p. 190-204.
53. Ahmed, N.M., et al., New eco-friendly anticorrosive core-shell pigments. Pigment & Resin Technology, 44(5): (2015) p. 276-291.
54. Ahmed, N.M., W.M. Abd El-Gawad, and E.R. Souaya, Study on the corrosion protection performance of new ferrite/kaolin core-shell pigments in epoxy-based paints. Anti-Corrosion Methods and Materials, 63(1): (2016) p. 36-46
55. Ahmed, N.M., et al., Electrochemical studies on the corrosion performance of new advanced anticorrosive pigments. Pigment & Resin Technology, 46(3): (2017) p. 181-193.